Effects of autoionizing resonances on electron-impact excitation rates and gain calculations for Ni-like tantalum

M. H. Chen and A. L. Osterheld
Lawrence Livermore National Laboratory, University of California, Livermore, California 94550
(Received 7 June 1995)

The electron-impact excitation-rate coefficients for the $3d$ to $4l$ transitions in Ni-like tantalum were calculated using the distorted-wave and the multiconfiguration Dirac-Fock methods. As for the few-electron cases, the effects of autoionizing resonances are found to be very important for most transitions. In some transitions, resonances can enhance the rate coefficients by as much as a factor of 5. A collisional-radiative model was employed to study the effects of resonances on the laser gains. We found that the inclusions of the resonance excitation-rate coefficients in the calculations significantly reduce the gain coefficients for the two $J=0\rightarrow 1$ lasing transitions but fail to explain the large discrepancies between the predicted and measured lasing spectrum.

PACS number(s): 34.80.Kw, 42.55.Vc

I. INTRODUCTION

Cross sections for electron-impact excitation of multiply charged ions are important for studies of high temperature plasmas related to astrophysics, fusion research, and x-ray laser design. In these applications, cross sections for many transitions and for several ion stages are usually required. To meet these vast demands, the distorted-wave approximation is frequently used to calculate electron collision cross sections. Electron-impact excitation, in general, can proceed through a direct-excitation channel or via autoionizing resonances. It has been shown that the autoionizing resonances can significantly enhance the calculated excitation rates especially for forbidden transitions [1–9]. Enhancements as large as a factor of 2 have been found for many different types of ions such as Li-like [3,4], Be-like [8], O-like [9], F-like [7], and Ne-like [5] ions. Hence, the neglect of resonance contributions in routine distorted-wave calculations could seriously underestimate the excitation-rate coefficients.

Ni-like tantalum ($Z=73$) has recently been demonstrated to achieve amplification in the soft x-ray regime by an electron collisional excitation scheme [10]. Since electron-impact excitation is the mechanism which produces the inversion, it is desirable to have good quality excitation cross sections in order to model the plasmas accurately. In this paper, we report calculations of resonance enhancement of the electron-impact excitation rates from the ground state to the $3d^9 4l$ excited states of Ni-like tantalum. The direct-excitation cross sections are calculated using the distorted-wave method. The resonance contributions are evaluated utilizing a two-step model. The required energy levels, Auger and radiative transition rates are computed using the multiconfiguration Dirac-Fock (MCDF) model [11,12]. We found resonance enhancements as large as a factor of 5 for many transitions. The primary effect of the resonance excitations is to reduce the calculated gain of the main Ni-like tantalum line at 44.83 Å.

II. THEORETICAL METHOD

An electron incident on a Ta^{45+} ion in its ground state can excite the ion and simultaneously be captured to form a doubly excited state of Ta^{44+}. The subsequent Auger decay to an excited state of the residual Ta^{45+} ion contributes to the excitation cross section from the ground to singly excited states of Ta^{45+}. For a Ni-like ion in the ground state, the direct-excitation (DE) process for $3d$ to $4l$ transitions can be represented by

$$e^- + 3s^2 3p^6 3d^{10} \rightarrow 3s^2 3p^6 3d^9 4l + e^- . \tag{1}$$

The resonance-excitation (RE) process with M-shell excitation can be described by

$$e^- + 3s^2 3p^6 3d^{10} \leftrightarrow 3l^{-1} n'l' n''l'' \rightarrow 3s^2 3p^6 3d^9 4l + e^- . \tag{2}$$

Here, the ten-electron neonlike core is ignored in the description of states in Eqs. (1) and (2). The notation $3l^{-1}$ indicates an electron is missing in the $3l$ shell.

In this work, the DE cross sections were evaluated using a relativistic distorted-wave approximation. The target wave functions were obtained from a relativistic configuration-interaction calculation with one-electron orbitals generated by a parametric potential [13]. The basis states include all states from the $3l^{-1}4l'$ and $3d^{-1}5l$ singly excited Ni-like manifolds. The contributions from the autoionizing resonances were computed separately from the DE processes. The resonance excitation was treated as a two-step process involving electron capture and then Auger decay to the excited state [14]. The effects of overlapping resonances and interference between DE and RE channels were neglected in these calculations.

Assuming a Maxwellian distribution of the plasma electrons, the total resonance-excitation-rate coefficients for a transition from a state i to state j is given by [14]

$$C_{ij}^{\mathrm{res}} = \sum_d C_{id}^{\mathrm{cap}} B_{dj}^{A} , \tag{3}$$

where the capture rate is obtained from the inverse Auger process by detailed balance:

$$C_{id}^{\rm cap}=(2g_i)^{-1}\left(\frac{4\pi R}{kT}\right)^{3/2}a_0^3\exp\left(-\frac{E_{di}}{kT}\right)g_d A_{di}^A, \quad (4)$$

and the Auger branching ratio is

$$B_{dj}^A=\frac{A_{dj}^A}{\Gamma_A(d)+\Gamma_r(d)}. \quad (5)$$

Here, a_0 and R are the Bohr radius and the Rydberg energy, respectively; g_i and g_d are the statistical weight factors; E_{di} and A_{di}^A are the Auger energy and Auger rate, respectively; and $\Gamma_A(d)$ and $\Gamma_r(d)$ are the total Auger and radiative rates for the autoionizing state d, respectively.

III. NUMERICAL CALCULATION

In the calculation of RE-rate coefficients [Eq. (2)], we explicitly include contributions from the intermediate states of $3s^23p^53d^{10}4lnl'$ $(n=5-9,l'\leq 4)$ and $3s^23p^63d^95lnl'$ $(n=5-9,l'\leq 4)$ configurations. The states from the first configuration can reach the $3d^94l$ singly excited states via $3p$-$3dnl$ Coster-Kronig transitions while those from the second configuration use the $4l$-$5lnl'$ Auger pathways. The contributions from high-n Rydberg states $(10\leq n\leq 50)$ were taken into account by using n^{-3} extrapolation of the transition rates.

Detailed Auger and electric-dipole radiative rates required in the calculations of the capture rates [Eq. (4)] and Auger branching ratios [Eq. (5)] were evaluated from perturbation theory using the MCDF model [11,12]. The energy levels and wave functions for the bound states were calculated in intermediate coupling with configuration interaction within the same complex by using the MCDF model in the average-level scheme [12].

IV. RESULTS AND DISCUSSION

A. The effects of resonances on excitation rates

The level identifications and energies for the $3d^94l$ states from the relativistic configuration-interaction calculations are listed in Table I. The levels are identified by their dominant components in the j-j coupled basis set. For simplicity, the Ar core is omitted in the identifications. In Table II, the calculated direct- and resonance-excitation-rate coefficients for Ta^{45+} from the ground state to 54 singly excited states in $3d^94l$ configurations are given for electron temperatures $400\leq T\leq 2500$ eV.

The direct- and resonance-excitation-rate coefficients for some selected low-lying excited states are compared in Figs. 1–6. The following observations can be made from these comparisons.

(i) For electron temperature $T<1000$ eV, the resonance contributions to the rate coefficients are larger than the direct excitation for most transitions. For example, the resonance rate for excited state 2 at $T=400$ eV is a factor of 5 larger than its direct rate coefficient.

(ii) For the electron temperatures in the range $100\leq T\leq 2500$ eV covered in this study, resonance excitations are as important as the direct excitation processes for most transitions.

TABLE I. Energy-level definitions for Ni-like tantalum.

Level no.	Identification	Energy (eV)
1	$3d^{10}$	0.0
2	$3d_{3/2}^4 3d_{5/2}^5 4sJ=3$	1506.1
3	$3d_{3/2}^4 3d_{5/2}^5 4sJ=2$	1508.0
4	$3d_{3/2}^3 3d_{5/2}^6 4sJ=1$	1568.2
5	$3d_{3/2}^3 3d_{5/2}^6 4sJ=2$	1569.5
6	$3d_{3/2}^4 3d_{5/2}^5 4p_{1/2}J=2$	1600.8
7	$3d_{3/2}^4 3d_{5/2}^5 4p_{1/2}J=3$	1602.2
8	$3d_{3/2}^3 3d_{5/2}^6 4p_{1/2}J=2$	1663.1
9	$3d_{3/2}^3 3d_{5/2}^6 4p_{1/2}J=1$	1666.4
10	$3d_{3/2}^4 3d_{5/2}^5 4p_{3/2}J=4$	1696.7
11	$3d_{3/2}^4 3d_{5/2}^5 4p_{3/2}J=2$	1698.5
12	$3d_{3/2}^4 3d_{5/2}^5 4p_{3/2}J=1$	1699.6
13	$3d_{3/2}^4 3d_{5/2}^5 4p_{3/2}J=3$	1701.7
14	$3d_{3/2}^3 3d_{5/2}^6 4p_{3/2}J=0$	1755.3
15	$3d_{3/2}^3 3d_{5/2}^6 4p_{3/2}J=1$	1759.9
16	$3d_{3/2}^3 3d_{5/2}^6 4p_{3/2}J=3$	1760.3
17	$3d_{3/2}^3 3d_{5/2}^6 4p_{3/2}J=2$	1762.9
18	$3d_{3/2}^4 3d_{5/2}^5 4d_{3/2}J=1$	1836.9
19	$3d_{3/2}^4 3d_{5/2}^5 4d_{3/2}J=4$	1842.2
20	$3d_{3/2}^4 3d_{5/2}^5 4d_{3/2}J=2$	1843.3
21	$3d_{3/2}^4 3d_{5/2}^5 4d_{3/2}J=3$	1845.7
22	$3d_{3/2}^4 3d_{5/2}^5 4d_{5/2}J=1$	1859.7
23	$3d_{3/2}^4 3d_{5/2}^5 4d_{5/2}J=5$	1861.4
24	$3d_{3/2}^4 3d_{5/2}^5 4d_{5/2}J=3$	1865.0
25	$3d_{3/2}^4 3d_{5/2}^5 4d_{5/2}J=2$	1866.1
26	$3d_{3/2}^4 3d_{5/2}^5 4d_{5/2}J=4$	1866.9
27	$3d_{3/2}^4 3d_{5/2}^5 4d_{5/2}J=0$	1880.0
28	$3d_{3/2}^3 3d_{5/2}^6 4d_{3/2}J=1$	1903.3
29	$3d_{5/2}^3 3d_{5/2}^6 4d_{3/2}J=3$	1903.7
30	$3d_{3/2}^3 3d_{5/2}^6 4d_{3/2}J=2$	1909.2
31	$3d_{3/2}^3 3d_{5/2}^6 4d_{5/2}J=1$	1921.6
32	$3d_{3/2}^3 3d_{5/2}^6 4d_{5/2}J=4$	1925.1
33	$3d_{3/2}^3 3d_{5/2}^6 4d_{5/2}J=2$	1926.6
34	$3d_{3/2}^3 3d_{5/2}^6 4d_{5/2}J=3$	1928.5
35	$3d_{3/2}^3 3d_{5/2}^6 4d_{3/2}J=0$	1948.2
36	$3d_{3/2}^4 3d_{5/2}^5 4f_{5/2}J=0$	2006.9
37	$3d_{3/2}^4 3d_{5/2}^5 4f_{5/2}J=1$	2010.1
38	$3d_{3/2}^4 3d_{5/2}^5 4f_{5/2}J=5$	2014.8
39	$3d_{3/2}^4 3d_{5/2}^5 4f_{5/2}J=2$	2015.0
40	$3d_{3/2}^4 3d_{5/2}^5 4f_{5/2}J=3$	2018.3
41	$3d_{3/2}^4 3d_{5/2}^5 4f_{7/2}J=6$	2018.4
42	$3d_{3/2}^4 3d_{5/2}^5 4f_{5/2}J=4$	2019.6
43	$3d_{3/2}^4 3d_{5/2}^5 4f_{7/2}J=2$	2019.7
44	$3d_{3/2}^4 3d_{5/2}^5 4f_{7/2}J=4$	2023.8
45	$3d_{3/2}^4 3d_{5/2}^5 4f_{7/2}J=5$	2025.3
46	$3d_{3/2}^4 3d_{5/2}^5 4f_{7/2}J=3$	2025.8
47	$3d_{3/2}^4 3d_{5/2}^5 4f_{7/2}J=1$	2038.2
48	$3d_{3/2}^3 3d_{5/2}^6 4f_{5/2}J=4$	2076.4
49	$3d_{3/2}^3 3d_{5/2}^6 4f_{5/2}J=2$	2077.5
50	$3d_{3/2}^3 3d_{5/2}^6 4f_{7/2}J=2$	2080.8
51	$3d_{3/2}^3 3d_{5/2}^6 4f_{7/2}J=5$	2083.0
52	$3d_{3/2}^3 3d_{5/2}^6 4f_{5/2}J=3$	2083.4
53	$3d_{3/2}^3 3d_{5/2}^6 4f_{7/2}J=3$	2085.9
54	$3d_{3/2}^3 3d_{5/2}^6 4f_{7/2}J=4$	2087.3
55	$3d_{3/2}^3 3d_{5/2}^6 4f_{5/2}J=1$	2104.5

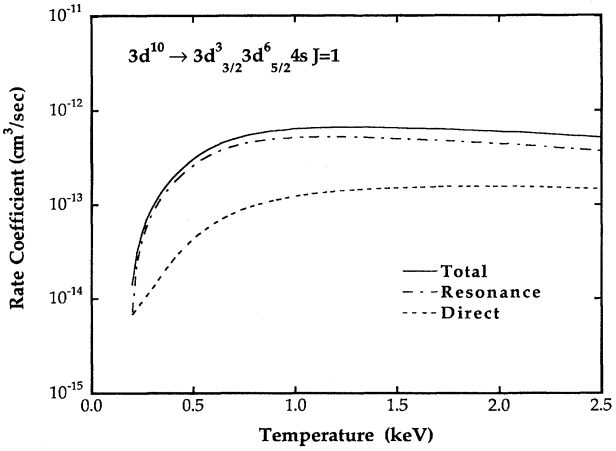

FIG. 1. Rate coefficients for the $3d^{10} \rightarrow 3d^3_{3/2}3d^6_{5/2}4sJ=1$ transition in Ta^{45+} as functions of electron temperature. The dashed curve represents the direct-excitation rates. The dash-dotted curve indicates the resonance contributions. The solid curve displays the total rate coefficients.

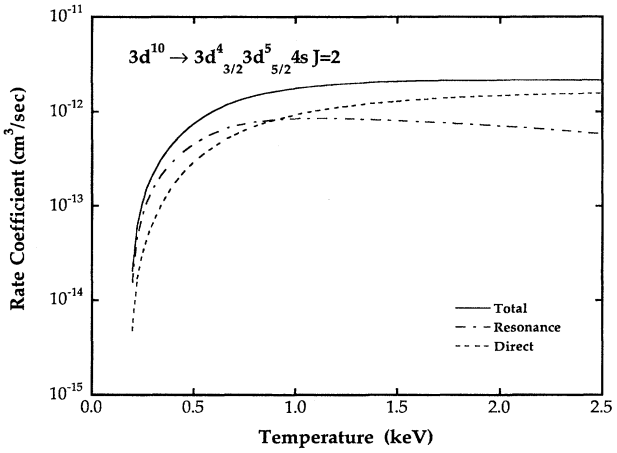

FIG. 2. Rate coefficients for the $3d^{10} \rightarrow 3d^4_{3/2}3d^5_{5/2}4sJ=2$ transition.

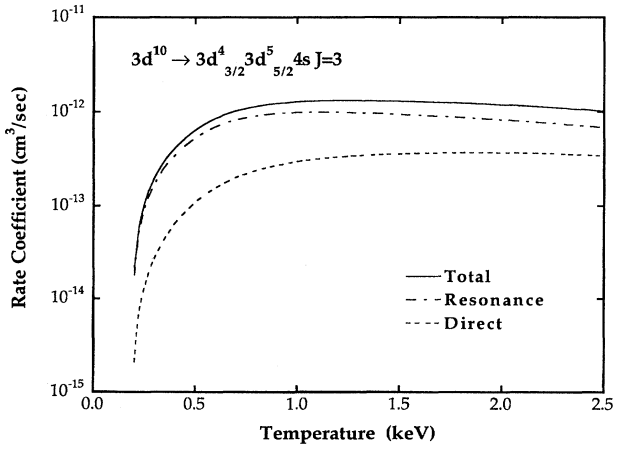

FIG. 3. Rate coefficients for the $3d^{10} \rightarrow 3d^4_{3/2}3d^5_{5/2}4sJ=3$ transition.

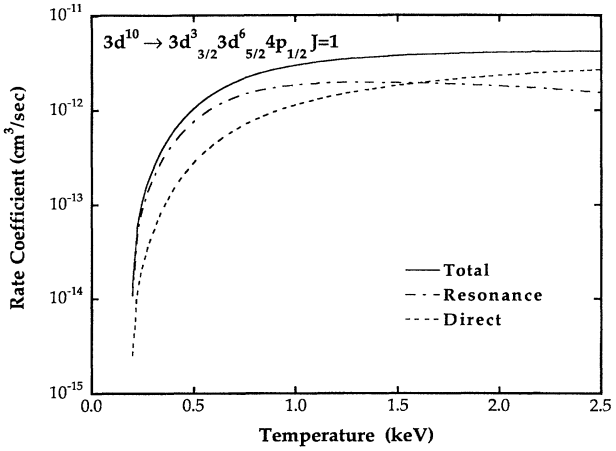

FIG. 4. Rate coefficients for the $3d^{10} \rightarrow 3d^3_{3/2}3d^6_{5/2}4p_{1/2}J=1$ transition.

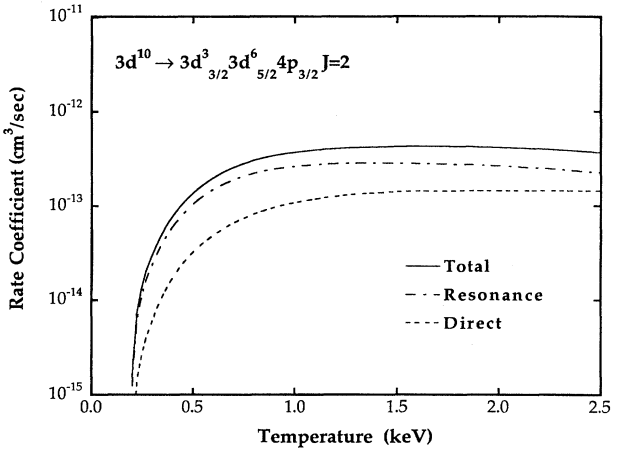

FIG. 5. Rate coefficients for the $3d^{10} \rightarrow 3d^3_{3/2}3d^6_{5/2}4p_{3/2}J=2$ transition.

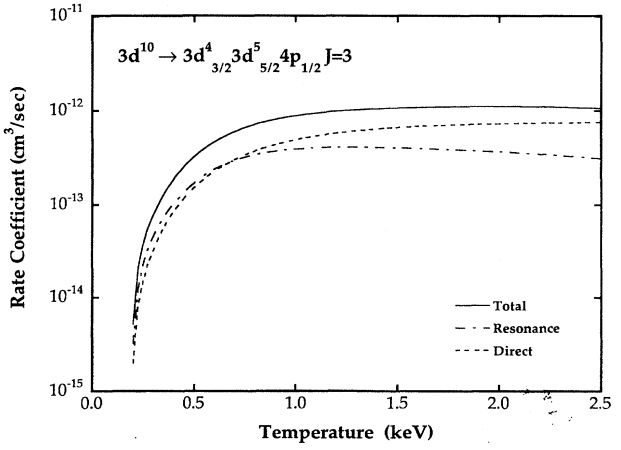

FIG. 6. Rate coefficients for the $3d^{10} \rightarrow 3d^4_{3/2}3d^5_{5/2}4p_{1/2}J=3$ transition.

TABLE II. Direct electron-impact excitation-rate coefficients (DE) and resonance contributions (RE) in 10^{-13} cm^3/sec from the ground state of Ni-like Ta.

Excited state		Electron temperature (eV) 400	800	1200	1500	2500	Excited state		Electron temperature (eV) 400	800	1200	1500	2500
2	DE	0.599	2.44	3.36	3.59	3.42	29	DE	0.365	2.44	3.93	4.48	4.70
	RE	3.44	9.26	9.99	9.42	6.82		RE	0.520	2.50	3.30	3.37	2.77
3	DE	1.49	7.12	11.2	13.0	15.8	30	DE	0.565	4.43	8.19	10.2	13.8
	RE	2.96	7.95	8.57	8.09	5.85		RE	0.507	2.40	3.14	3.20	2.63
4	DE	0.225	0.991	1.40	1.51	1.46	31	DE	0.283	1.95	3.20	3.68	3.93
	RE	1.63	4.74	5.27	5.01	3.69		RE	0.585	2.76	3.61	3.68	3.01
5	DE	0.927	4.68	7.41	8.67	10.5	32	DE	0.395	2.79	4.67	5.46	6.16
	RE	2.60	7.65	8.51	8.13	6.02		RE	0.557	2.81	3.77	3.87	3.23
6	DE	0.406	1.90	2.75	3.01	2.97	33	DE	0.402	2.98	5.22	6.28	7.69
	RE	1.02	3.46	4.06	3.95	3.03		RE	0.754	3.85	5.19	5.34	4.46
7	DE	0.757	3.78	5.81	6.65	7.51	34	DE	0.244	1.67	2.70	3.09	3.23
	RE	0.986	3.47	4.12	4.03	3.10		RE	0.526	2.70	3.63	3.74	3.12
8	DE	0.329	1.63	2.39	2.62	2.58	35	DE	11.2	90.2	167	207	272
	RE	0.831	3.09	3.73	3.67	2.86		RE	0.909	5.13	7.14	7.46	6.34
9	DE	1.25	8.00	14.5	18.3	26.9	36	DE	0.190	1.44	2.43	2.83	3.06
	RE	4.12	16.1	19.7	19.5	15.3		RE	0.101	0.583	0.814	0.850	0.726
10	DE	0.502	2.61	3.88	4.30	4.30	37	DE	0.476	3.32	5.39	6.24	10.7
	RE	0.891	3.33	4.03	3.97	3.09		RE	0.230	1.38	1.95	2.04	1.76
11	DE	0.253	1.33	2.00	2.23	2.25	38	DE	0.333	2.63	4.61	5.50	6.48
	RE	0.663	2.56	3.12	3.10	2.43		RE	0.261	1.52	2.12	2.21	1.89
12	DE	1.56	10.7	20.1	25.9	38.8	39	DE	0.463	3.52	5.91	6.84	7.33
	RE	4.35	16.0	19.2	18.8	14.6		RE	0.327	1.94	2.74	2.87	2.46
13	DE	0.310	1.76	2.83	3.30	3.85	40	DE	0.370	2.86	4.88	5.72	6.37
	RE	0.588	2.33	2.87	2.85	2.25		RE	0.338	2.01	2.84	2.97	2.55
14	DE	0.080	0.458	0.709	0.799	0.827	41	DE	0.500	3.80	6.37	7.36	7.85
	RE	0.177	0.731	0.913	0.912	0.725		RE	0.345	2.06	2.91	3.06	2.62
15	DE	0.253	1.66	2.90	3.57	4.81	42	DE	0.245	1.84	3.05	3.51	3.68
	RE	1.02	4.10	5.05	5.03	3.97		RE	0.316	1.88	2.64	2.77	2.38
16	DE	0.420	2.55	4.19	4.91	5.77	43	DE	0.358	2.73	4.57	5.28	5.63
	RE	0.875	3.56	4.43	4.42	3.50		RE	0.464	2.71	3.80	3.96	3.38
17	DE	0.148	0.832	1.27	1.42	1.44	44	DE	0.363	2.77	4.63	5.34	5.68
	RE	0.546	2.26	2.82	2.83	2.24		RE	0.308	1.84	2.58	2.71	2.32
18	DE	0.449	2.80	4.44	5.04	5.29	45	DE	0.206	1.58	2.68	3.12	3.46
	RE	0.586	2.49	3.13	3.14	2.51		RE	0.359	2.12	2.98	3.12	2.67
19	DE	0.519	3.32	5.41	6.26	7.00	46	DE	0.681	6.16	11.9	15.1	20.7
	RE	0.493	2.15	2.75	2.76	2.23		RE	0.494	2.92	4.10	4.30	3.68
20	DE	0.498	3.29	5.50	6.47	7.59	47	DE	9.04	87.8	178	233	344
	RE	0.605	2.61	3.31	3.32	2.67		RE	1.23	7.67	11.0	11.6	10.0
21	DE	0.318	1.97	3.08	3.47	3.55	48	DE	0.273	2.23	3.82	4.46	4.82
	RE	0.507	2.29	2.94	2.98	2.41		RE	0.288	1.86	2.68	2.84	2.48
22	DE	0.302	1.92	3.07	3.48	3.65	49	DE	0.401	3.30	5.71	6.69	7.30
	RE	0.648	2.80	3.56	3.58	2.88		RE	0.348	2.29	3.33	3.54	3.10
23	DE	0.613	3.88	6.15	6.96	7.21	50	DE	0.306	2.52	4.35	5.09	5.54
	RE	0.584	2.69	3.49	3.53	2.89		RE	0.276	1.81	2.64	2.80	2.46
24	DE	0.381	2.42	3.85	4.36	4.52	51	DE	0.252	2.16	3.88	4.67	5.58
	RE	0.655	3.03	3.93	4.00	3.26		RE	0.271	1.74	2.51	2.66	2.32
25	DE	0.850	6.31	11.4	14.2	18.8	52	DE	0.267	2.49	4.77	6.00	8.05
	RE	0.687	3.06	3.93	3.98	3.22		RE	0.343	2.22	3.21	3.41	2.98
26	DE	0.295	1.90	3.05	3.50	3.77	53	DE	0.430	3.94	7.43	9.25	12.1
	RE	0.504	2.35	3.06	3.11	2.54		RE	0.360	2.29	3.31	3.51	3.06
27	DE	1.80	13.4	24.0	29.4	37.7	54	DE	0.199	1.62	2.77	3.22	3.44
	RE	1.09	5.61	7.56	7.80	6.52		RE	0.319	2.06	2.98	3.15	2.75
28	DE	0.246	1.65	2.68	3.07	3.25	55	DE	23.5	248	518	686	1040
	RE	0.560	2.66	3.49	3.56	2.92		RE	1.22	8.16	12.0	12.8	11.3

(iii) For the strongest transitions such as $1 \rightarrow 55 (3d^{10} \rightarrow 3d^3_{3/2} 3d^6_{5/2} 4f_{5/2} j = 1)$, resonances contribute only a few percent to the excitation-rate coefficients.

(iv) Resonance-excitation rates peak around $T = 1200$ eV while the direct-excitation rates reach their maxima at much higher temperatures. As temperature increases, the importance of the resonances slowly diminishes.

B. The effects on plasma gain

There are several puzzles in the observed Ni-like tantalum lasing spectrum [10,15]. A number of transitions are predicted to have significant gain coefficients, the three main predicted lasing transitions are the $3d^3_{3/2} 3d^6_{5/2} 4d_{3/2} J = 0 \rightarrow 3d^3_{3/2} 3d^6_{5/2} 4p_{1/2} J = 1$ transition at 44.83 Å (levels 35–9 using the level list in Table I), the $3d^3_{3/2} 3d^6_{5/2} 4d_{3/2} J = 0 \rightarrow 3d^4_{3/2} 3d^5_{5/2} 4p_{3/2} J = 1$ transition at 50.97 Å (levels 35–12) and the $3d^4_{3/2} 3d^5_{5/2} 4d_{5/2} J = 2 \rightarrow 3d^4_{3/2} 3d^5_{5/2} 4p_{3/2} J = 1$ transition at 74.42 Å (levels 25–12). Only the 44.83-Å transition is observed to have measurable gain. This is particularly puzzling since the 44.83- and 50.97-Å lines have the same upper state. Typical conditions of the gain region in the Ni-like tantalum experiments were electron temperatures near 1000 eV, and electron densities of approximately 10^{21} cm^{-3}. For these conditions, the lower laser levels have populations per degeneracy roughly $\frac{1}{3}$ as large as the upper levels and the gain coefficients are sensitive to the population mechanisms of both the upper and lower levels. Since the resonances produce large enhancements of collisional excitation rates, it is important to investigate their effects in the gain calculations.

The inversions on the two $J = 0 \rightarrow 1$ transitions are produced by the strong monopole excitation of the metastable $J = 0$ level and the fast radiative decay of the lower levels. The population of the upper level is almost totally produced by the ground-state excitation rate. As shown in Table II, the resonances contribute little to the direct excitation of the upper level for temperatures near 1000 eV, but strongly enhance the ground-state excitation rate of the lower levels. Thus the resonance-excitation process should reduce the calculated gain for these transitions. The situation for the $J = 2 \rightarrow 1$ transition is more complicated, since the upper-level population is produced by several excitation, recombination, and cascade processes.

The effect of the resonance-excitation process was investigated quantitatively with the use of a collisional-radiative model of V-like through Ga-like tantalum ions similar to the model described in [15]. Steady-state gain coefficients were calculated with and without the additional resonance-excitation contributions. These calculations treated the plasma as optically thin, assumed that the electron and ion temperatures were identical, and used Voight profiles which included collisional decays in the natural lifetime. Results of these calculations are given in Table III as a function of temperature for ion densities of 2×10^{19} and 2×10^{20} cm^{-3}. The lower density is typical of the plasma experiments in [10], while the higher density is roughly the density where the steady-state gain coefficients are maximum for temperatures near 1000 eV. The calculations at this higher density were motivated by proposals to use short-wavelength, short-pulse pump lasers to produce higher density, higher gain plasma amplifiers [16].

TABLE III. Gain coefficients for predicted Ni-like tantalum lasing transitions, calculated with and without the effect of resonance excitation. For each temperature, the row labeled RE includes the resonances and the row labeled DE does not. The lasing transitions are labeled following [15].

		Gain coefficients (cm^{-1})					
		$N_{ion} = 2 \times 10^{19}$ cm^{-3}			$N_{ion} = 2 \times 10^{20}$ cm^{-3}		
T_e (eV)		A [a]	B [b]	F [c]	A [a]	B [b]	F [c]
600	DE	0.23	0.18	0.20	4.36	4.30	0.92
	RE	0.20	0.17	0.30	1.25	2.79	0.80
800	DE	1.96	1.57	2.11	21.4	20.8	8.73
	RE	1.71	1.46	2.71	11.2	15.0	8.66
1000	DE	4.75	3.90	5.94	26.0	25.4	14.1
	RE	4.10	3.54	6.88	15.8	18.9	13.3
1200	DE	5.84	4.90	8.24	17.1	17.0	11.1
	RE	4.99	4.36	8.89	11.4	13.2	10.4
1400	DE	5.12	4.38	7.99	8.76	8.86	6.54
	RE	4.40	3.90	8.31	6.32	7.18	6.16
1600	DE	3.83	3.34	6.50	4.08	4.19	3.38
	RE	3.33	3.00	6.65	3.10	3.51	3.22
1800	DE	2.64	2.34	4.83	1.84	1.92	1.67
	RE	2.33	2.12	4.89	1.46	1.65	1.60
2000	DE	1.74	1.56	3.39	0.84	0.89	0.82
	RE	1.56	1.43	3.42	0.68	0.78	0.79

[a] $3d^3_{3/2} 3d^6_{5/2} 4d_{3/2} J = 0 \rightarrow 3d^3_{3/2} 3d^6_{5/2} 4p_{1/2} J = 1$ transition (44.83 Å).
[b] $3d^3_{3/2} 3d^6_{5/2} 4d_{3/2} J = 0 \rightarrow 3d^4_{3/2} 3d^5_{5/2} 4p_{3/2} J = 1$ transition (50.97 Å).
[c] $3d^4_{3/2} 3d^5_{5/2} 4d_{5/2} J = 2 \rightarrow 3d^4_{3/2} 3d^5_{5/2} 4p_{3/2} J = 1$ transition (74.31 Å).

The resonance-excitation process reduces the gain of the two $J = 0 \rightarrow 1$ transitions by 10–15 %, for temperatures near 1000 eV and an ion density of 2×10^{19} cm^{-3}. This reduction is smaller than might be expected from the dramatic enhancement of the excitation rate to the lower levels. The reason is that only a small part of the population of either of the lower levels is produced by its ground-state excitation rate, while the rest is mainly produced by cascades from other levels. Many of the cascade contributions arise from levels excited either by monopole excitations or recombination processes. Neither of these processes is affected much by resonance excitation. The resonances have a much larger effect up to 50% reduction for $J = 0 \rightarrow 1$ transitions at the higher ion density, 2×10^{20} cm^{-3}. As collisional mixing drives the level populations towards local thermodynamic equilibrium, the enhancements in the lower-level populations become larger fractions of the inversions. Finally, the inclusion of resonance excitation does not help explain the absence of the second $J = 0 \rightarrow 1$ line at 50.97 Å. The predicted gain on this transition is reduced less by the resonance-excitation process than the gain on the observed laser line at 44.83 Å.

At the lower ion density, the resonances increase the predicted gain of the $J = 2 \rightarrow 1$ transition at 74.42 Å by 10–15 % for temperatures near 1000 eV. This is because the resonance-excitation process, including the effects of cascades, increases the population of the upper level more than the lower level. As the density is increased, collisional mix-

ing reduces the enhancement in the gain coefficient. At an ion density of 2×10^{20} cm^{-3}, the resonances produce a small reduction in the predicted gains. As for the $J=0\rightarrow1$ transitions, the resonances do not explain the absence of observed gain for this transition.

V. CONCLUSIONS

In summary, we have calculated the direct- and resonance-excitation-rate coefficients for the $3d$ to $4l$ transitions in Ni-like tantalum. As for the few-electron cases, we found that the effects of autoionizing resonances are significant for most transitions. In some cases, autoionizing resonances can enhance the rate coefficients by as much as a factor of 5. We conclude once again that the autoionizing resonances play an important role in the calculation of electron-impact excitation cross sections and rate coefficients for Ni-like ions.

These excitation rates were used in a collisional-radiative model to estimate gain coefficients for Ni-like tantalum. These calculations demonstrated important effects of the resonances on calculated gains, but did not explain the large discrepancies between the predicted and measured lasing spectrum.

ACKNOWLEDGMENT

This work was performed under the auspices of the U.S. Department of Energy by Lawrence Livermore National Laboratory under Contract No. W-7405-ENG-48.

[1] R. J. W. Henry, Phys. Rep. **6**, 1 (1981).
[2] A. K. Pradhan, D. W. Norcross, and D. G. Hummer, Phys. Rev. A **23**, 619 (1981); Astrophys. J. **246**, 1031 (1981).
[3] K. Bhadra and R. J. W. Henry, Phys. Rev. A **26**, 1848 (1981).
[4] R. E. H. Clark, A. L. Merts, J. B. Mann, and L. A. Collins, Phys. Rev. A **2**, 1812 (1983).
[5] K. J. Reed and A. Hazi (unpublished).
[6] M. S. Pindzola, D. C. Griffin, and C. Bottcher, Phys. Rev. A **32**, 822 (1985).
[7] K. J. Reed, M. H. Chen, and A. U. Hazi, Phys. Rev. A **36**, 3117 (1987).
[8] M. H. Chen and B. Crasemann, Phys. Rev. A **37**, 2886 (1988).
[9] K. J. Reed, M. H. Chen, and A. U. Hazi, Phys. Rev. A **38**, 3319 (1988).
[10] B. J. MacGowan, S. Maxon, L. B. Da Silva, D. J. Fields, C. J. Keane, D. L. Matthews, A. L. Osterheld, J. H. Scofield, G. Shimkaveg, and G. F. Stone, Phys. Rev. Lett. **65**, 420 (1990).
[11] M. H. Chen, Phys. Rev. A **31**, 1449 (1985).
[12] I. P. Grant *et al.*, Comput. Phys. Commun. **21**, 207 (1980); B. J. Mckenzie *et al.*, *ibid.* **21**, 233 (1980).
[13] M. Klapisch, J. L. Schwob, B. S. Fraenkel, and J. Oreg, J. Opt. Soc. Am. **61**, 148 (1977); A. Bar-Shalom, M. Klapisch, and J. Oreg, Phys. Rev. A **38**, 1773 (1988).
[14] R. D. Cowan, J. Phys. B **13**, 1471 (1980).
[15] A. L. Osterheld, B. K. Young, R. S. Walling, W. H. Goldstein, J. H. Scofield, M. H. Chen, G. Shimkaveg, M. Carter, R. Shepherd, B. J. MacGowan, L. Da Silva, D. Matthews, S. Maxon, R. London, and R. E. Stewart, in *X-ray Lasers 1992*, Third International Colloquium, Schliersee, edited by E. E. Fill, IOP Conf. Ser. No. 125 (Institute of Physics and Physical Society, London, 1992), p. 309.
[16] M. H. Key, in *X-ray Lasers, 1992* (Ref. [15]), p. 171.